Bounds for interpolating complex effective moduli of viscoelastic materials from measured data

D. J. Eyre*†, G. W. Milton† and R. S. Lakes‡

August 5, 1999

Abstract

The complex effective moduli of viscoelastic materials can be experimentally measured by a number of techniques giving relaxation data for materials at discrete frequencies. In this paper, we present a method which allows one to find bounds on the moduli of the material at the unmeasured frequencies. Our bounds can be very tight, and are therefore, good approximations to the data. Using our bounds, experimentalists can concentrate their efforts on gathering highly accurate data at only a few frequencies and numerically generate data at other frequencies that may be of interest.

Keywords: Viscoelasticity, complex moduli, relaxation, bounds

*corresponding author, eyre@math.utah.edu, tel: 1 801 582-4052, FAX: 1 801 585 1640
†Department of Mathematics, University of Utah, Salt Lake City, UT 84112 USA
‡Department of Engineering Physics, University of Wisconsin, Madison, WI 53706 USA

1 Introduction

The physical reality of viscoelastic behavior may be represented mathematically by a variety of functions of time or frequency. The complex dynamic function of frequency is regarded as most closely related to direct perception. All these functions are interrelated, see for example Gross (1947, 1968); most of the exact relationships are integral transforms. For example, the transient time dependent functions which describe creep (strain response to step stress) or relaxation (stress response to step strain) are related to the dynamic functions which describe the response to sinusoidal input, by a one-sided sine or cosine Fourier transform. For the complex dynamic moduli, the real and imaginary parts are related by the Kramers-Kronig relations, Kronig (1926) and Kronig and Kramers (1928), which are integral transforms.

Frequency-dependent data must be taken at close intervals if there is any possiblity of resonance, since resonant behavior gives rise to sharp peaks in the dynamic structural properties. In measurements of relaxing systems on the continuum scale one does not expect resonance provided the frequency in question is sufficiently below the lowest natural frequency of the microstructure. It is the purpose of this paper to explore the question of the required density of data points to properly characterize relaxing systems, and to elucidate the question of inferences one can make for frequencies higher or lower than those available in the data. The upper frequency limit is dictated by experimental limitations such as resonance in the apparatus. The lower frequency limit is usually dictated by the patience of the experimenter.

At all but the highest frequencies, the response of many linear viscoelastic materials can be well approximated by a relaxation model, which neglects micro-inertial effects in the stress-strain relation for the material itself, possibly a composite. The macroscopic force-displacement relation for a structural element will exhibit structural resonance even in the absence of micro-resonance. For example, consider a complex effective modulus $G^*(p) = G'(p) + iG''(p) = |G^*(p)|e^{i\delta(p)}$ as a function of angular frequency $p = i\omega$ for an isotropic viscoelastic material. The relaxation model says this function has the integral representation, Schwarzl and Struik (1967),

$$G^*(p) = \int_0^\infty \frac{H(\tau)d\tau}{1+p\tau} \tag{1}$$

where $H(\tau)$ is a positive real-valued distribution function of relaxation times τ and $p = p_1 + ip_2$ is a complex frequency. Here τ is called the relaxation time.

The function $G^*(p)$ is analytic in the entire complex plane with possible exceptions on the negative real p-axis. Additionally, the function is positive and real on the positive real p-axis, has positive real part for $p_1 > 0$, and finally, $G^*(p) = \overline{G(\bar{p})}$, where the bar denotes complex conjugation.

Often experimental data for $G^*(p)$ are analysed by making some additional assumptions about $H(\tau)$. Commonly used models include fitting the data to a delta function spectrum or to a box function spectrum. In the latter case, the box spectrum function, Tobolsky (1960), is taken to be

$$H(\tau) = \begin{cases} H_0 & \text{if } \tau_1 \le \tau \le \tau_2 \\ 0 & \text{otherwise} \end{cases} \tag{2}$$

and then the data is used to try to fit the positive parameters τ_1, τ_2 and H_0.

Rather than making these ad-hoc assumptions about the form of $H(\tau)$, this paper provides bounds on $G^*(p)$ given its measured values $G(p_j)$ at N-frequencies, $p_1, p_2, \ldots, p_N$. We refer to these frequencies as *anchor points.* Our bounds interpolate these data values and bound $G^*(p)$ at values of p where G has not been measured. Moreover, the bounds we provide are the *sharpest possible* within the class of functions compatible with functions that can be represented by the integral given in (1), and the bounds provide *analytically admissible approximants* to the experimental data.

Specifically this paper addresses the question: given that one knows how a material responds to oscillatory inputs at a set of N frequencies, what bounds can one place on its response at another frequency?

The mathematical techniques used to produce the bounds are based on the observation that $G^*(p)$ is a Stieltjes function of p. Then finding bounds on $G^*(p)$ amounts to finding bounds on a Stieltjes function given its value at n points in the complex plane. Mathematically, the problem has been solved by Milton (1981), (see also Baker (1969), who analysed the case where the n points were located on the positive real p-axis, and Bergman who provided the alternative derivation in Bergman (1993). The bounds are a lens shaped region in the complex plane for every value of p.

The lens shaped regions are described as the intersection of two circles that are given by rational functions (having a discrete relaxation spectrum) that are compatible with the data and which have one free parameter. Determining these two circles in the complex plane involves varying their free parameters independently while interpolating the known data values. In this paper, we describe the rational functions that define the bounds, and give examples of their use to bound data.

The remainder of this paper is divided into three sections. In §2, the bounds are used to bound and approximate the moduli of materials that have box relaxation spectra, and used to bound and approximate experimental relaxation data for an alloy made from cadmium and magnesium. In §3, we describe the bounds and their calculation, and we give a brief justification of them. Finally in §4, we describe how the bounds can be used by experimentalists to obtain data at unmeasured frequencies.

2 Examples of the use of the bounds

The practical utility of our bounds will be demonstrated with two sets of examples. In the first set of examples, the bounds are applied to model problems with box relaxation spectra. In the second set of examples, the bounds are applied to experimentally obtained data describing the relaxation of cadmium-magnesium alloys.

2.1 The bounds applied to model spectra

If the relaxation spectra are a sum of delta functions, the material moduli corresponding to these types of spectra are rational functions, Gross (1969). Our bounds are themselves rational and they interpolate the data provided. Therefore, if the number of data points that are being interpolated is sufficiently large, our bounds will exactly recover the complex moduli of these materials.

Our bounds are applied to model problems with box relaxation spectra in Figures 1–2. The material moduli corresponding to the spectrum are

$$G'(p) = \frac{H_0}{2} \log \left(\frac{1 + p^2 \tau_2^2}{1 + p^2 \tau_1^2} \right) \tag{3}$$

and

$$G''(p) = H_0 \left[\tan^{-1}(\tau_2 p) - \tan^{-1}(\tau_1 p) \right]. \tag{4}$$

When our bounds are applied to a box whose support is small, i.e. box spectrum that approximates a delta spectrum, the resulting bounds are very tight because our bounds can exactly recover the delta function. Even when the support of the box is large, the bounds are reasonably tight as seen in Figure 1. Here we take $H_0 = 1$, $\tau_1 = 0.01$ and $\tau_2 = 100$. We use two points to anchor our bounds, at $p_1 = 0.1i$ and $p_2 = 10i$ and show the bounds for both the real and imaginary parts of G.

In all of this paper's figures, the anchors are easy to find since they are the points where the bounds interpolate the data.

In figure 2, we take a spectrum composed of two disjoint boxes. The first box has $H_0 = 1$, $\tau_1 = 0.1$ and $\tau_2 = 0.5$ and the second box has $H_0 = 10$, $\tau_1 = 20$ and $\tau_2 = 24$. The sum of the spectrum with these two boxes are qualitatively different than the single boxes. Two anchor points, at $p_1 = 0.1i$ and $p_2 = 2i$, for our bounds are used. The bounds are tight again, and with only two anchors, the bounds capture the apparent inflection points in $G'(p)$ and the two maxima and the minimum of $G''(p)$.

PUT FIGURES 1 and 2 HERE

2.2 The bounds applied to cadmium-magnesium data

In this section, the bounds are applied to experimentally obtained viscoelastic properties of cadmium-magnesium alloys. The alloy used and the experiments performed to obtain these data are described in Cook and Lakes (1995). In Figures 3-5, we take two, three and four anchor points, respectively, and we show how incorporating more information by including more anchors can tighten the bounds.

In Figure 3, experimentally obtained data and a set of two point bounds are shown. These bounds were generated by using the experimental data with anchors taken at 0.1 and 5.62 Hz. No other information from the experimental data was used to generate these bounds. Figure 3(a) shows the bounds for $\tan\delta = G''/G'$ and Figure 3(b) shows the bounds for $|G|$. Notice that all but one of the measurements of $\tan\delta$ are consistent with the bounds, and all but three measurements of $|G|$ are consistent with the bounds, and in each of these cases, the deviation of the data from the bounds is less than the error estimates for the experimental results.

When the data and their errors are outside the bounds, there are two possibilities. First, the measurements at the anchors contain enough error to produce inconsistent bounds, or second, the bounds reflect the fact that the remaining data are not perfect. We now address the case where the anchors contain errors. In Figure 4 we study errors in the two anchor points at 0.1 and 5.62 Hz with a Monte-Carlo simulation. We generated with random normally distributed errors with mean zero and a 10% standard deviation and computed the bounds for 30 samples. Figure 4(a) shows the maximum upper and minimum lower bounds for $\tan\delta$ and Figure 4(b) shows the maximum upper and minimum lower bounds for $|G|$ in the presence of the random errors. More anchors will tighten these bounds, but if the deviation of the bounds exceeds error estimates, then one would do well to seek sources of error not accounted for initially.

In Figure 5, experimentally obtained data and a set of three point bounds are shown. These bounds were generated by using the experimental data with anchors taken at 0.01, 0.1 and 5.62 Hz. Figure 5(a) shows the bounds for $\tan\delta$ and Figure 5(b) shows the bounds for $|G|$. Notice that by adding the new anchor, the bounds are tightened at lower frequencies.

In Figure 6, experimentally obtained data and a set of four point bounds are shown. These bounds were generated by using the experimental data with anchors taken at 0.01, 0.1, 5.62 and 31.62 Hz. Figure 6(a) shows the bounds for $\tan\delta$ and Figure 6(b) shows the bounds for $|G|$. In these bounds, either the accuracy of both $\tan\delta$ and $|G|$ of several of the data vales between 1 and 10 Hz should be questioned or the accuracy of the anchor values should be questioned. If the anchor values are assumed to be correct, then these four point bounds could be used to approximate the data at intermediate frequencies.

PUT FIGURES 3 – 6 HERE

3 A description and justification of the bounds

To describe the bounds, suppose that $G^*(p)$ has been measured at N frequencies on the negative imaginary p-axis. Because the complex moduli satisfy the symmetry property $G^*(p) = \overline{G^*(\bar{p})}$, these N measurements allow us to incorporate data at $2N$ frequencies into the bounds.

The bounds are rational functions that interpolate the known $2N$ data points, and that are consistent with the integral representation of the complex moduli given in (1.1). It will be shown below that the rational functions that satisfy these requirements are one of the following two possibilities:

- The first rational function interpolates the data, and has N simple poles and N simple zeros interlaced along the negative real axis with a zero closest to the origin. None of the poles are located at the origin and none of the zeros are located at infinity. Otherwise, the positions of the poles and zeros and the amplitude of the candidate function, a total of $2N + 1$ parameters, are partially determined by the $2N$ known values leaving one parameter free. This parameter is varied, keeping frequency fixed, to determine one of the two circles defining the bounds in the complex plane at the given frequency.

- The second rational function interpolates the data, has N simple poles and N simple zeros interlaced along the negative real axis, and has one additional pole at $p = 0$ and one additional zero at $p = \infty$. Again, the positions of the poles and zeros and the amplitude of the function, a total of $2N + 1$ parameters, are partially determined by the $2N$ known values leaving one parameter free. This parameter is varied, keeping frequency fixed, to determine the second circle defining the bounds in the the complex plane.

The two circles intersect in the complex plane, and their intersection is a lens shaped region for every frequency. At any frequency $\hat{p}$, the real and imaginary bounds on $G(\hat{p})$ are the minimum and maximum of the real and imaginary parts of the lens shaped region at the frequency $\hat{p}$. The bounds on $|G|$ and $\tan\delta$ are obtained from the maximum and minimum values of these quantities over the boundary of the lens shaped region.

The justification of these bounds rests on a straightforward extension of the analysis in Milton (1981). There bounds were derived on the complex effective permittivity ϵ_e of a composite with two isotropic phases with permittivities ϵ_1 and ϵ_2, given values of the function $\epsilon_e(\epsilon_1, \epsilon_2)$ at N points (see also McPhedran and Milton (1981) where the bounds were numerically computed and tested). The derivation was based on the fact that $G^*(p) = \epsilon_e(1/p, 1)$ is a Stieltjes function of p, satisfying $G^*(1) = 1$. The proof given there is easily adapted to the present case where one does not know the value of $G^*(1)$.

The bounds on G' and G'' are not necessarily analytic and must be computed numerically. To do this, we express the numerator and denominator of the bounds as polynomials using a power basis. We choose the leading order coefficient of the denominator to be one and we choose the leading order coefficient of the numerator to be our free parameter. Let $\mathcal{G}_i(p)$ denote the ith bound, and in the first bound, the degrees of the numerator and denominator are equal, so

$$\mathcal{G}_1(p) = \frac{\sum_{i=0}^{N} a_i p^i}{\sum_{i=0}^{N} b_i p^i}, \tag{5}$$

The second bound that has a pole at the origin and a zero at infinity, so the degree of the denominator is $N+1$, and

$$\mathcal{G}_2(p) = \frac{\sum_{i=0}^{N} \alpha_i p^i}{p \sum_{i=0}^{N} \beta_i p^i}. \tag{6}$$

The second bound has a zero at $p = \infty$ if $\beta_N \neq 0$, and has a pole at $p = 0$ if $\alpha_0 \neq 0$.

The remaining coefficients of the polynomials are then determined by the constraint that the bounds interpolate the data,

$$\mathcal{G}_i(p_j) = G(p_j), \quad \text{for } j = 1, 2, \ldots, 2N. \tag{7}$$

This provides a set of linear equations for these coefficients. This set of equations has

$2N+1$ unknowns and $2N$ equations, and its solutions determine the circle in the complex plane described above. Values on the circle are determined by two steps. First, fixing one coefficient and solving for the remaining $2N$ coefficients with the $2N$ equations determines the rational function $\mathcal{G}_2(p)$. Then evaluating the bound at a frequency gives a point on the circle.

To completely define the circle, one must know its center and radius. Since points on the circle are equally spaced from the center, only three points on the circle are needed to determine it. Two of these three points are easy to determine. These points occur where second bound coincides with the first bound, so in fact, these two points are shared by both circles. These points are defined as the points where the second bound takes the two special cases described above, i.e. first that $\beta_N = 0$, and second that $\alpha_0 = 0$. These are also special cases of the first bound, where $b_0 = 0$ and where $a_N = 0$, respectively. Thus these points are shared by the two circles, and are the intersection points.

One point on each bound must still be determined. Unfortunately, finding a point that is sufficiently far from the two known points to numerically find the circle is not easy because the points on the bounding circles do not change much over large ranges of the free parameter. Our approach was to choose the leading order coefficient of the numerator as our free parameter. For each value of the free parameter, we compute a point on the circle, and then we numerically maximize the sum of the distances between that point and the two points we already know. This maximization problem has two local maximums, and so long as the point we find allows us to accurately determine the circles, we accept either value. To numerically maximize the distance, we use the Nelder-Mead algorithm, for example see Dennis and Woods (1987).

4 Conclusions

As our examples demonstrate, the bounds can be very tight, even when only a few data points are incorporated. This should allow experimentalists to simplify their method of measurement since they should now need far less data to obtain equal results. Alternatively, an experimentalist could use our bounds in combination with their data to detect when the relaxation model breaks down. Even when the relaxation model breaks down $G'(p)$ and $G''(p)$ should still be compatible with the bounds derived in Milton *et. al.* (1997).

Our bounds are not as strong when the anchor points are at widely spaced frequencies. In this case, the bounds diverge rapidly at high frequencies above the data and low frequencies below the data. Furthermore, the bounds require more data to become tight enough to use as a reasonable approximation to the data at the unmeasured frequencies.

Acknowledgments

The work of GWM and DJE was supported by the General Motors Corporation and the National Science Foundation through grants DMS-9803748, DMS-9629692 and DMS-9402763. The work of RSL was supported by the National Science Foundation through grant CMS-9896284.

References

[1] Baker, G.A. (1969) Best error bounds for Padé approximants to convergent series of Stieltjes, J. Math. Phys. **10**, 814–820

[2] Bergman, D.J. (1993) Hierarchies of Stieltjes functions and their application to the calculation of bounds for the dielectric constant of a two-component composite medium, SIAM J. Appl. Math., **53**, 915–930

[3] Cook, L.S. and Lakes, R.S. (1995) Viscoelastic spectra of Cd0.67Mg0.33 in torsion and bending, Met. Trans, **26A**, 2037–2039

[4] Dennis, J.E. and Woods, D.J., in New Computing Environments: Microcomputers in Large-Scale Computing, edited by A. Wouk, SIAM, (1987).

[5] Gross B. (1947) On creep and relaxation, J. Appl. Phys. **18**, 212–221

[6] Gross B. (1968) Mathematical Structure of the Theories of Viscoelasticity, Hermann, Paris

[7] Kronig, R. (1926) On the theory of dispersion of X-rays, J. Opt. Soc. Am, **12**, 547–555

[8] R. Kronig, and H. A. Kramers (1928) Zur Theorie der Absorption und dispersion in den Röntgenspektren, in German, Z. Physik, **48**, 174–179

[9] McPhedran, R.C. and Milton, G.W. (1981) Bounds and exact theories for the transport properties of inhomogeneous media, Appl. Phys. A, **26**, 207–220

[10] Milton, G.W. (1981) Bounds on the transport and optical properties of two-componenet composite materials, J. Appl. Phys. **52**, 5294–5304

[11] Milton, G.W., Eyre, D.J., and Mantese, J.V. (1997) Finite Frequency Kramers Kronig Relations: Bounds on the Dispersion, Phys. Rev. Lett., **79**, 3062–3065

[12] Schwarzl, F.R. and Struik, L.C.E. (1967) Analysis of relaxation measurements, Advan. Mol. Relaxation Processes, **1**, 201–255

[13] Tobolsky, A. B. (1960) Properties and Structure of Polymers, J. Wiley, NY

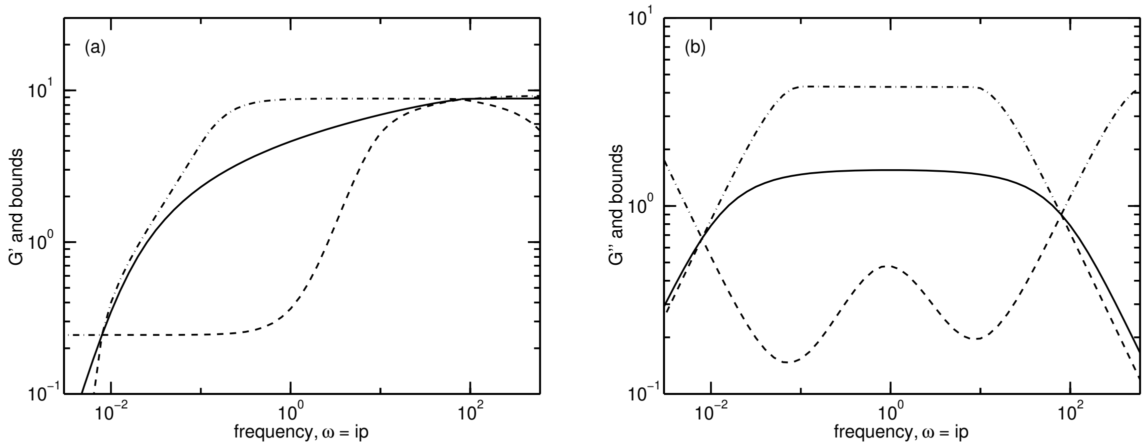

Figure 1: Real and imaginary parts of the material moduli with its upper and lower bounds where the materials distribution function is defined by a box spectrum. These bounds were generated using only 2 data points.

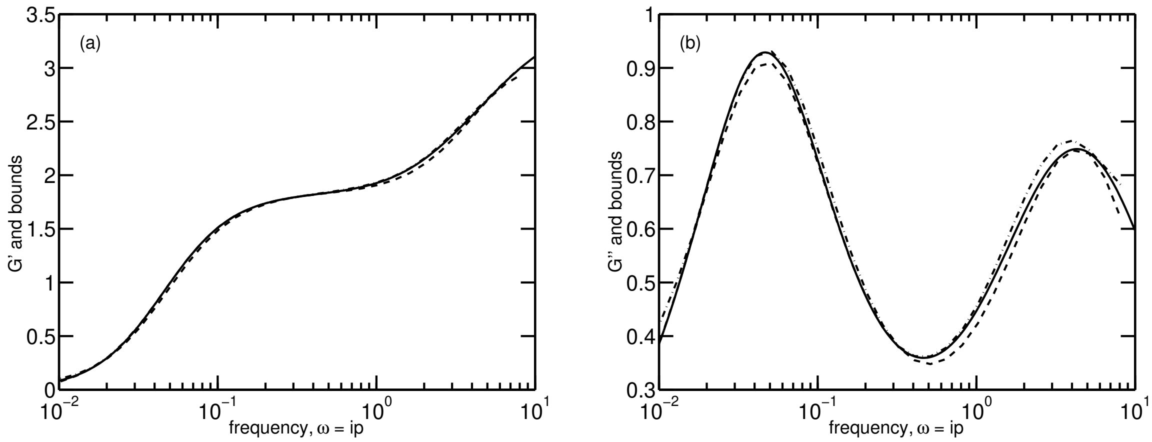

Figure 2: Real and imaginary parts of the material moduli with its upper and lower bounds where the materials distribution function is defined by two box spectra. These bounds were generated using 3 data points. We have found similar results when the anchors are chosen closer together as well.

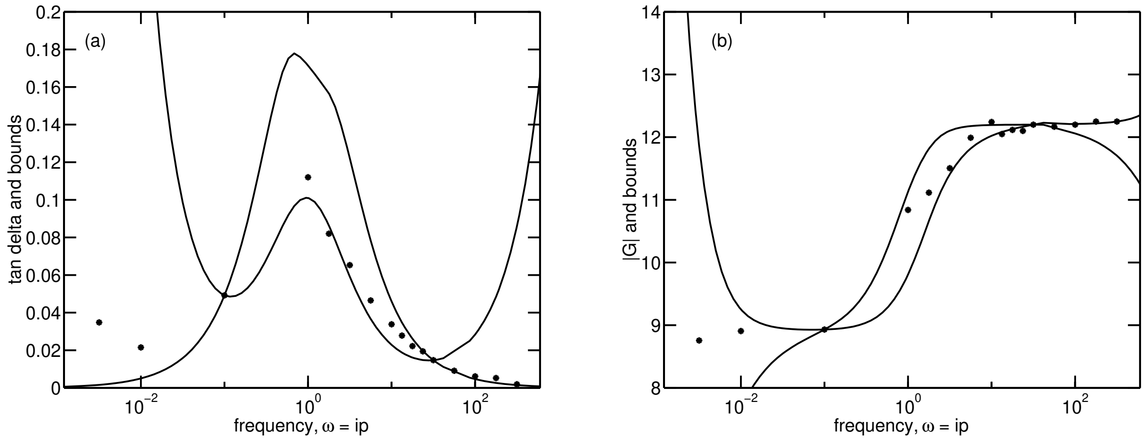

Figure 3: Data and two point $\tan\delta$ and $|G|$ bounds for cadmium-magnesium alloys. The anchors are taken at 0.1 Hz and 5.62 Hz. Figure 3(a) shows the bounds for $\tan\delta$ and Figure 3(b) shows the bounds for $|G|$.

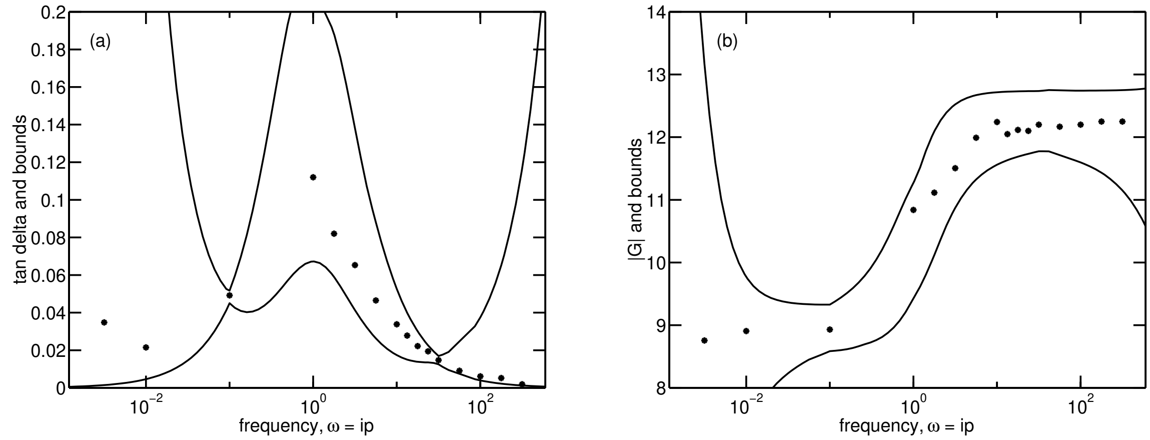

Figure 4: Data and two point $\tan\delta$ and $|G|$ bounds for cadmium-magnesium alloys with errors added to the data at the anchor points. The anchors are taken at 0.1 Hz and 5.62 Hz. Figure 4(a) shows the bounds for $\tan\delta$ and Figure 4(b) shows the bounds for $|G|$.

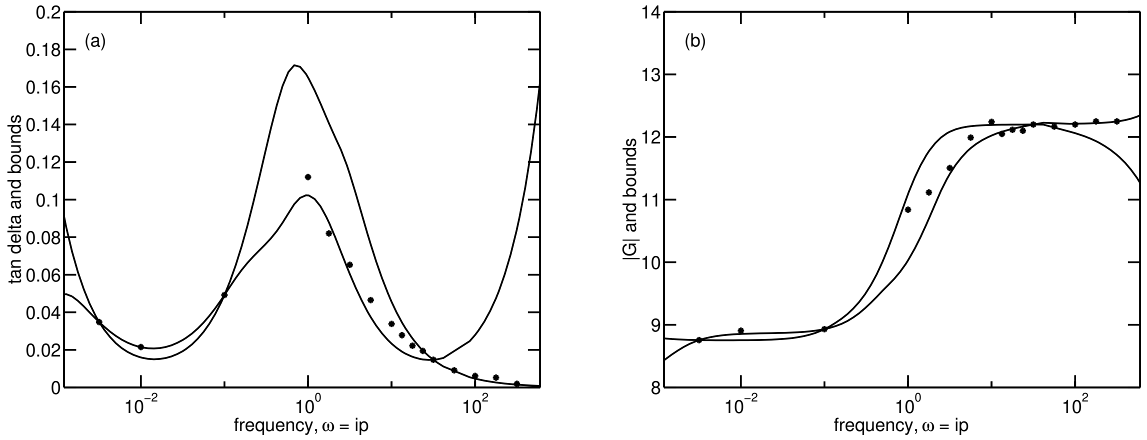

Figure 5: Data and three point $\tan\delta$ and $|G|$ bounds for cadmium-magnesium alloys. The anchors are taken at 0.01, 0.1 and 5.62 Hz. Figure 5(a) shows the bounds for $\tan\delta$ and Figure 5(b) shows the bounds for $|G|$.

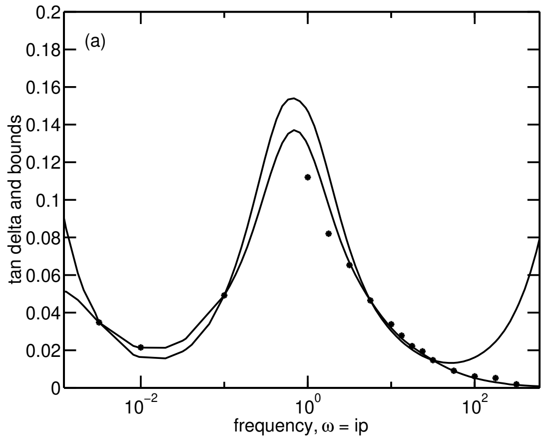

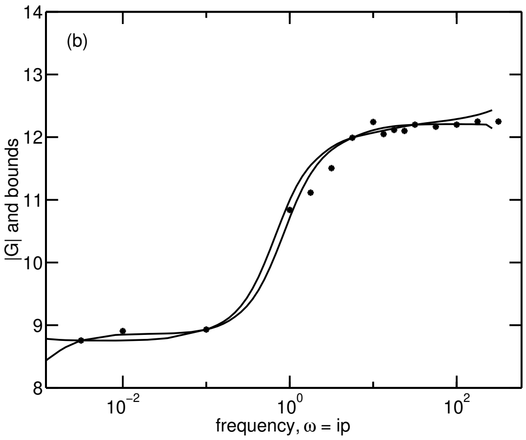

Figure 6: Data and four point $\tan\delta$ and $|G|$ bounds for cadmium-magnesium alloys. The anchors are taken at 0.01, 0.1, 5.62 and 31.62 Hz. Figure 6(a) shows the bounds for $\tan\delta$ and Figure 6(b) shows the bounds for $|G|$.